Applied Catalysis B: Environmental 91 (2009) 92–100

Contents lists available at ScienceDirect

Applied Catalysis B: Environmental

journal homepage: www.elsevier.com/locate/apcatb

Effect of hydrothermal treatment and silica on thermal stability and oxygen storage capacity of ceria–zirconia

Vadivukarasi Raju, Stephan Jaenicke, Gaik-Khuan Chuah *

Department of Chemistry, National University of Singapore, 3 Science Drive 3, Kent Ridge, Singapore 117543, Singapore

ARTICLE INFO

Article history:
Received 11 February 2009
Received in revised form 28 April 2009
Accepted 9 May 2009
Available online 19 May 2009

Keywords:
Ceria–zirconia
Hydrothermal treatment
Oxygen storage capacity
Thermal stability
Silica doping

ABSTRACT

Hydrothermal digestion of freshly precipitated cerium–zirconium hydroxides was used to synthesize nanocrystalline ceria–zirconia. This simple method produced ceria–zirconia with higher surface area and thermal stability than the untreated oxide. After calcination at 1000 °C, the surface area of the hydrothermally synthesized samples was ~11–12 m^2/g while the untreated $Ce_{0.5}Zr_{0.5}O_2$ had only 4.2 m^2/g. The continuous dissolution and reprecipitation of hydroxides during hydrothermal treatment is postulated to a more defect-free structure which is able to withstand loss of surface area when exposed to high temperatures. In addition, these nanocrystalline oxides were more reducible than the untreated oxide. While the addition of silica to ceria–zirconia further increased the surface area and oxygen storage capacity, the oxides suffered severe loss of surface area after calcination to 1000 °C. A silica-rich overlayer was formed which decreased the oxygen storage capacity as compared to silica-free ceria–zirconia. The oxygen storage capacity shows a strong dependence on the surface area for values below 50 m^2/g but diffusion of oxygen from the bulk becomes limiting for high surface area ceria–zirconia.

1. Introduction

Ceria-based oxides are widely used in three-way automotive catalytic converters as support material and as an oxygen promoter [1]. In order to simultaneously remove carbon monoxide and hydrocarbons as well as nitrogen oxides, a narrow range of air-to-fuel ratio near stoichiometric amounts must be maintained. Ceria acts as an oxygen buffer for the three-way catalysts by releasing and taking up oxygen through the Ce^{4+}/Ce^{3+} couple ($CeO_2 \leftrightarrow CeO_{1.5} + 0.25O_2$). This ensures that the local atmosphere at the catalyst surface remains stoichiometric even when the air-to-fuel ratio in the engine changes so that a high NO_x conversion can be achieved. However, pure ceria is not suitable because of its low oxygen storage capacity (OSC) and poor thermal stability [2,3]. To improve the thermal stability, metal ions are normally introduced into ceria [4–14]. In particular, the insertion of zirconium ions into ceria was found to be extremely beneficial in terms of thermal stability and oxygen storage [15–20]. It is believed that the distortion of the metal–oxygen bonds results in a highly mobile lattice oxygen species, so that the reduced zone is not confined to the surface layers but extends deep into the bulk [21,22]. Mamontov et al. [23] postulated that substitution of the smaller Zr^{4+} ion gives rise to strain in the mixed oxide, which can be alleviated by the promotion of Ce^{4+} to Ce^{3+} ions (ionic radius of 97 pm vs. 128 pm, respectively). Some EXAFS studies have been interpreted that in $Ce_{0.5}Zr_{0.5}O_2$, the Zr^{4+} assumes a sixfold rather than an eightfold coordination where two of the oxygen atoms are located at a nonbonding distance [17]. These "non-bonded" oxygens are believed to be responsible for the high oxygen mobility. However, Lemaux et al. [20] used a three-cumulant expansion approach in the analysis of the EXAFS data, and concluded that four short intralayer Zr–O and four longer interlayer Zr–O bonds are present in $Ce_{0.5}Zr_{0.5}O_2$. They proposed that the latter oxygens are labile and hence, contribute to the enhancement of oxygen storage capacity in the mixed oxides. Contrary to these findings, Nagai et al. [24] found that in an atomically homogeneous $Ce_{0.5}Zr_{0.5}O_2$ sample, all eight Zr–O bonds are symmetric. As this sample had the highest OSC compared to two other oxides which showed tetragonal and distorted tetragonal structures, the authors proposed that the enhancement in OSC arose from homogeneity in the mixing of Ce and Zr atoms which in turn facilitate the Ce^{4+} to Ce^{3+} valence change. Further improvement in the OSC can be obtained by incorporating trivalent metals such as Al^{3+}, Y^{3+}, La^{3+} or Ga^{3+} into the ceria–zirconia solid solution [25–28]. Doping with rare earth metals such as lanthanum, praseodymium, neodymium and yttrium was found to effectively stabilize the metastable tetragonal t''-phase, which is a defect structure containing oxygen vacancies and interstitials [29].

* Corresponding author. Tel.: +65 6516 2839; fax: +65 6779 1691.
E-mail address: chmcgk@nus.edu.sg (G.-K. Chuah).

0926-3373/$ – see front matter © 2009 Elsevier B.V. All rights reserved.
doi:10.1016/j.apcatb.2009.05.010

With regulations requiring lower emission standards, adjustment to fuel combustions have resulted in higher temperature of emissions [30]. Hence, different strategies have been used to form ceria–zirconia with improved high thermal stability and durability. These include coprecipitation from the salts [31,32], sol–gel [33], micro-emulsion [34], and dry ball milling [35]. Kim et al. [36] claimed that continuous hydrothermal synthesis in supercritical water produced ceria–zirconia with higher thermal stability and reducibility than oxides prepared by coprecipitation. The preparation by flame spray synthesis is another route producing high surface areas up to 80 m^2/g after calcination at 900 °C [37]. However, despite this, the OSC was lower than that of samples prepared by coprecipitation. Supported ceria–zirconia was found to be highly resistant to sintering under reduction–oxidation treatment [30,38]. Furthermore, the small particles of a ceria-rich phase at the surface of the support are believed to be responsible for enhanced low temperature reducibility [38–42].

We have previously found that high surface area zirconia could be prepared by digestion of the hydrous precursor at 100 °C in an alkaline medium [43–45]. The surface area of the resulting zirconia increased with digestion time. However, it was later realized that during digestion, silica from the glassware was inadvertently incorporated into the zirconia, where it aided the stabilization of the surface area. Nevertheless, subsequent studies using Teflon apparatus showed that the digestion of the precursor hydrous oxide, either by open reflux or hydrothermal treatment in a closed vessel, was indeed able to enhance the thermal stability and surface area of the formed oxide [46]. In the present study, we investigate the preparation of ceria–zirconia by hydrothermal treatment on the precursor hydroxides and compare their textural and redox properties with the untreated oxide. As silica has been reported to enhance the OSC [47], its effect on the hydrothermally treated ceria–zirconia is studied. Furthermore, the correlation of surface area and OSC is investigated as some authors have reported that OSC is closely related to the surface area [48] while others found that it has little or no influence on the OSC [24,29,49]. For example, Nagai et al. [24] reported that a $Ce_{0.5}Zr_{0.5}O_2$ sample with 1 m^2/g exhibited a higher OSC than samples with surface areas of 89 and 125 m^2/g. In a study of $Ce_{0.2}Zr_{0.8}O_2$ prepared by different synthesis routes, Kašpar et al. [49] suggested that the lack of correlation between the surface area and dynamic OSC, indicates the involvement of subsurface or bulk oxygen even under dynamic conditions.

2. Experimental

2.1. Preparation of samples

Ceria, zirconia and mixed oxides with cerium:zirconium ratio of 1:3, 1:1 and 3:1 were prepared by coprecipitation. Zirconium tetrachloride and ammonium cerium nitrate were dissolved together in deionized water to form a 0.2 M solution of each salt. The solution was slowly added, with stirring, via a peristaltic pump to an excess of 5 M ammonia solution. After the addition was completed, the pH was adjusted to 9.5 and the suspension was refluxed at 100 °C for 2 days in a Teflon round-bottom flask. The precipitate was filtered, washed, dried at 100 °C and calcined at 500 °C for 12 h. A heating ramp of 5 °C min^{-1} was used to reach the final temperature. The samples are labeled as C_1Z_3-*R*-2, *CZ*-*R*-2 and C_3Z_1-*R*-2 where *R* stands for reflux, and 2 the days of reflux. For the hydrothermal treatment, the freshly precipitated cerium–zirconium (1:1) hydroxide together with the mother liquor was placed in Teflon-lined autoclaves and heated at 100 °C for 1, 2, 4, and 8 days. An aliquot was set aside without any hydrothermal treatment. The calcined samples are labeled as *CZ*-*H*-*t* where *H* stands for hydrothermal synthesis and *t* = 0, 1, 2, 4 and 8 days. Silica-containing $Ce_{0.5}Zr_{0.5}O_2$ was prepared as follows: after coprecipitation of the cerium–zirconium hydroxide, tetraethylorthosilicate (TEOS) was added to the mother liquor to achieve the desired silicon loading (1–10 wt.%) and the sample was hydrothermally treated at 100 °C in a Teflon-lined autoclave for 4 days. These samples are denoted as *x%Si-CZ-H*-4 where *x%* denotes the wt.% of Si and *H* represents hydrothermal synthesis. In another series, the length of hydrothermal treatment on 4%Si–$Ce_{0.5}Zr_{0.5}O_2$ was studied. The calcined samples are designated as 4%Si-CZ-H-*t*, where *t* = days of hydrothermal treatment.

2.2. Characterization

The crystalline phases of the samples were determined by powder X-ray diffraction using a Siemens D5005 diffractometer equipped with a copper anode (λ: 0.15418 nm), operated at 40 kV and 40 mA. The 2θ range from 20° to 70° (step size 0.02°, dwell time 1 s) was measured. The average crystallite size was calculated from the Scherrer equation using a smaller step size of 0.004° for the 2θ range from 26° to 34°. Multipoint BET surface area and adsorption/desorption isotherms were determined from nitrogen adsorption at −196 °C (Micromeritics Tristar 3000). Prior to the measurements, the samples were degassed at 300 °C under a flow of N_2 for 6 h. The pore size distribution was calculated from the desorption isotherm using the Barrett, Joyner and Halenda method. Elemental analysis for cerium, zirconium and silicon was determined by ICP-AES after dissolution in hydrofluoric acid. X-ray photoelectron (XPS) spectroscopy was used to determine the surface elemental composition. The measurements were made in a VG Escalab MkII using a Mg Kα X-ray source (1253.6 eV, 300 W). The binding energies are calibrated to the carbon 1 s peak of CH at 284.6 eV. The peak areas were determined after peak fitting and normalized with the manufacturer's atomic sensitivity factors for the different elements [50].

2.3. Temperature programmed reduction (TPR) and oxygen storage capacity (OSC)

The calcined samples were first pretreated at 700 °C for 2 h in a flow of helium (50 ml min^{-1}). After cooling to room temperature, the gas was switched to 10% CO in helium (total flow 30 ml min^{-1}) and the CO and CO_2 signals were monitored by a quadrupole mass spectrometer (Balzers Prisma 200) as the sample was heated to 700 °C at 10 °C min^{-1}. After the sample had been reduced, the reactor was flushed with helium for 1 h before pulses of oxygen were introduced using a 250 μl sample loop. The oxygen storage capacity (OSC) at 700 °C was estimated from the number of pulses required before an oxygen signal was detected. The reoxidized sample was cooled to 600 °C in flowing helium, and CO gas was introduced to the sample. The CO signal in the gas leaving the reactor was monitored by the mass spectrometer until it returned to baseline, whereupon reduction of the sample was considered complete. The sample was then flushed with helium for an hour, and oxygen pulses were introduced to reoxidize the sample. The same procedure was repeated at 500 and 400 °C. The weight changes during CO reduction and oxidation were also measured by a microbalance in a thermogravimetry analyzer (Mettler-Toledo Star^e).

3. Results and discussion

3.1. Variation of cerium:zirconium ratio on textural properties

Samples of pure ceria, ceria–zirconia (Ce:Zr of 3:1, 1:1 and 1:3), and zirconia were prepared by calcination at 500 °C of the respective hydroxides that had been subjected to reflux for 2 days.

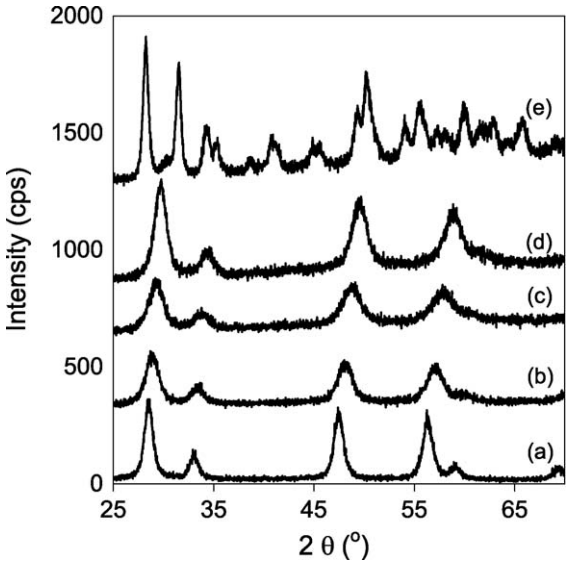

Fig. 1. XRD patterns of (a) CeO_2-R-2, (b) C_3Z_1-R-2, (c) C_1Z_1-R-2, (d) C_1Z_3-R-2 and (e) ZrO_2-R-2.

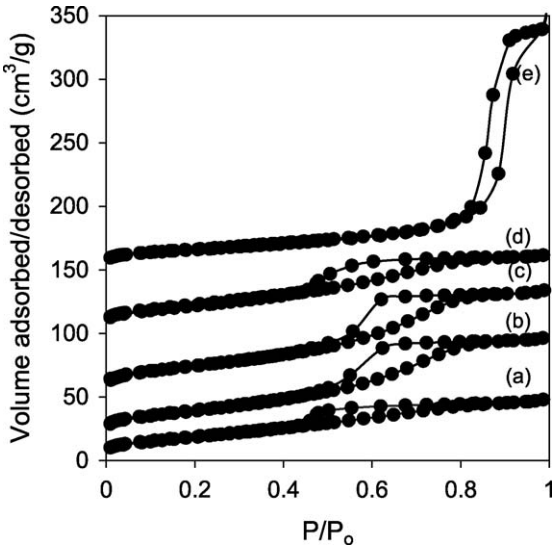

Fig. 2. Nitrogen sorption isotherms of (a) CeO_2-R-2, (b) C_3Z_1-R-2, (c) C_1Z_1-R-2, (d) C_1Z_3-R-2 and (e) ZrO_2-R-2.

The X-ray diffraction patterns showed that the calcined samples crystallized in the cubic fluorite-type phase (Fig. 1). However, ceria–zirconia samples with the formula $Ce_xZr_{1-x}O_2$ (x between 0.35 and 0.65) have also been reported to form the metastable tetragonal phases, t' or t'', both belonging to the space group $P4_2/nmc$ [21,22,34]. The t' phase is formed through a diffusionless phase transition with c/a in the range of 1.001–1.02, while the pseudo-cubic t'' has a structure very close to that of the cubic phase. Because of the nanocrystalline nature of the materials, the observed peak widths are very broad, ~1.7°, making it impossible to discern the presence of the metastable tetragonal phases where the expected splitting constants are of the order of 0.5°. However, there is a displacement of the diffraction peaks to higher 2θ with increasing zirconium loading. The lattice parameter, a, decreased from 5.4132 Å in CeO_2-R-2 to 5.1860 Å in C_1Z_3-R-2. The decrease is due to substitution of the larger 8-coordinated Ce^{4+} (ionic radius 97 pm) by the smaller Zr^{4+} ion (ionic radius 84 pm) [51]. The isotonic decrease in the lattice parameter with zirconium content is in accordance with Vegard's rule for the formation of solid solutions [52]. Unlike the ceria–zirconia samples, pure zirconia crystallized predominantly in the monoclinic phase. The average crystallite size, D, was calculated from the width of the (1 1 1) peak at 2θ ~29.5° using the Scherrer equation, $D = K\lambda/\beta\cos\theta$, where the constant K is taken as 0.9, and β is the peak line width corrected for instrumental broadening. The average crystallite size was between 5.8 and 6.8 nm while unsubstituted ceria formed bigger crystallites around 10 nm (Table 1).

The BET surface areas of the calcined ceria–zirconia samples were between 81 and 89 m^2/g, which is higher than for CeO_2-R-2 or ZrO_2-R-2. From the nitrogen sorption isotherms (Fig. 2), a H2 type hysteresis loop associated with ill-defined pores was measured for CeO_2-R-2 [53]. Using the Barrett, Joyner and Halenda (BJH) equation, the pore diameter was calculated to be 3–4 nm. In comparison, the isotherms of the ceria–zirconia samples show wider hysteresis with pore diameters in the range of 3–5 nm. The nitrogen adsorption and desorption branches for ZrO_2-R-2 are nearly parallel and vertical from P/P_0 0.8–0.98. This H1 type hysteresis is typically found in agglomerates of spheroidal particles of rather uniform size and array [53].

3.2. Oxygen storage capacity of $Ce_xZr_{1-x}O_2$-R-2

The OSC was estimated by injecting oxygen pulses to the reduced sample at 700 °C, until there was no further increase in the intensity of the oxygen signal. During the initial pulses, the mass spectrometer detected some CO_2 (between 0.01 and 0.03 mmol/g). This shows that during TPR with CO, some carbon was formed on the surface of the oxide. The dissociation and/or disproportionation of CO have been observed to occur over partially reduced ceria

Table 1
Textural properties of pure ceria–zirconia samples calcined at 500 °C.

Sample	Surface area (m^2/g)	Pore vol. (cm^3/g)	Crystallite size (nm)[a]		Ce/Zr[b] (mol:mol)
			Before TPR	After TPR	
CeO_2-R-2	57.1	0.07	10.2	18.7	–
C_3Z_1-R-2	89.3	0.10	6.5	8.1	2.53
C_1Z_1-R-2	88.5	0.13	5.8	6.2	1.07
C_1Z_3-R-2	81.3	0.13	6.8	7.5	0.26
ZrO_2-R-2	69.6	0.31	–	–	–
CZ-H-0	59.2	0.06	5.5	7.4	1.07
CZ-H-1	93.3	0.11	5.6	7.0	1.08
CZ-H-2	94.6	0.12	5.4	6.5	1.08
CZ-H-4	128	0.15	4.9	5.9	1.09
CZ-H-8	130	0.16	5.0	5.8	1.09

[a] Calculated from Scherrer equation.
[b] From ICP-AES.

Table 2
Oxygen storage capacity at 700 °C for ceria–zirconia samples.

Sample	OSC (mmol O_2/g)	Sample	OSC (mmol O_2/g)	
	From O_2 pulsing		From O_2 pulsing	From TGA
CeO_2-R-2	0.37	CZ-H-0	0.50	0.49
C_3Z_1-R-2	0.54	CZ-H-1	0.59	
C_1Z_1-R-2	0.58	CZ-H-2	0.58	
C_1Z_3-R-2	0.44	CZ-H-4	0.56	0.58
ZrO_2-R-2	–	CZ-H-8	0.57	
0%Si-CZ-H-4	0.57	4%Si-CZ-H-0	0.50	0.50
1%Si-CZ-H-4	0.64 (0.65)[a]	4%Si-CZ-H-1	0.55	
2%Si -CZ-H-4	0.63 (0.64)	4%Si-CZ-H-2	0.59	
3%Si-CZ-H-4	0.64 (0.66)	4%Si-CZ-H-4	0.65	
4%Si-CZ-H-4	0.65 (0.68)	4%Si-CZ-H-8	0.69	0.70
5%Si-CZ-H-4	0.65 (0.68)			
7.5%-Si-CZ-H-4	0.58 (0.61)			
10%Si-CZ-H-4	0.55 (0.58)			

[a] In parenthesis, OSC per g of $Ce_{0.5}Zr_{0.5}O_2$.

even at room temperatures [54]. The oxygen consumed for the titration of the surface carbon was deducted from the total oxygen uptake. As pure zirconia did not undergo any measurable reduction, no oxygen uptake was noted (Table 2). The OSC for ceria at 700 °C was 0.37 mmol O_2/g, showing that about 25% of the cerium participated in the Ce^{4+}/Ce^{3+} redox reaction. The value is within the range of 0.186–0.50 mmol O_2/g reported by other groups [23,55]. The OSC of the ceria–zirconia samples was higher than that of pure ceria, between 0.44 and 0.58 mmol O_2/g. Using these OSC values and the cerium content per mole of $Ce_{1-x}Zr_xO_2$ (x = 0.25–0.75), the fraction of cerium ions participating in the redox reaction was calculated to be 46–95%. The highest OSC of 0.58 mmol O_2/g was measured in C_1Z_1-R-2 (Table 2). Sugiura [12] attributed the enhanced oxygen storage at 50 mol% ZrO_2 to the formation of a κ-phase $CeZrO_4$ where Ce^{4+} and Zr^{4+}ions are regularly arranged. The close proximity of the smaller Zr^{4+} to Ce^{4+}allows lattice expansion to occur easily when Ce^{4+} is reduced to Ce^{3+}. It is also likely that the equimolar Ce:Zr ratio represents a balance of oxygen vacancies and interstitial oxygens as the zirconium content in the mixed oxide increased. Both the oxygen vacancies (tetrahedral holes normally occupied by the oxide ions) as well as the interstitial oxygen (at octahedral sites) are important in the oxygen storage property [23,48]. The incorporation of zirconium into ceria has been reported by Mamontov et al. [23] to result in oxygen deficiency. Using neutron diffraction and Rietveld refinement, these authors found that the total oxygen content in ceria was close to stoichiometry, but in ceria–zirconia, up to 7–8% more oxygen vacancies than interstitial oxygen were present.

3.3. *Effect of hydrothermal treatment on textural properties of $Ce_{0.5}Zr_{0.5}O_2$*

A series of cerium–zirconium (1:1) hydroxides was prepared and hydrothermally treated at 100 °C instead of being subjected to open reflux. Our previous studies have shown that open reflux and hydrothermal synthesis at 100 °C yielded zirconia with very similar textural properties. The duration of hydrothermal treatment on the structure and stability of the resulting oxides was investigated. The XRD peaks of the 500 °C-calcined $Ce_{0.5}Zr_{0.5}O_2$ are broad and highly symmetrical (Fig. 3). Small crystallites were formed in samples hydrothermally treated for 4 and 8 days as compared to the untreated oxide (Table 1). ICP-AES measurements show that the cerium:zirconium ratio agrees quite closely with the expected values.

The nitrogen adsorption studies revealed that the untreated sample, CZ-H-0, has low pore volume and a narrow pore size distribution centered around 3.4 nm (Fig. 4). Hydrothermally treated samples have a wider range of pore sizes from ~4 to 5.6 nm and bigger pore volumes than CZ-H-0. The porosity increased from 0.06 cm^3/g in CZ-H-0 to 0.16 cm^3/g for hydrothermally treated samples (Table 1). After calcination at 500 °C for 12 h, the $Ce_{0.5}Zr_{0.5}O_2$ obtained from the untreated hydroxide had a surface area of 59 m^2/g. Hydroxides that had been subjected to hydrothermal treatment at 100 °C formed oxides with higher surface areas, ranging from 94 to 130 m^2/g. After calcination to 700 °C, the surface area of the untreated sample, CZ-H-0, decreased to 33 m^2/g but hydrothermally treated oxides had surface areas of 52–97 m^2/g (Fig. 5). The surface areas were quite stable and did not change significantly even after four reduction–oxidation cycles at 700 °C. Even after calcination at 1000 °C, the hydrothermally treated samples still retained surface areas of ~9–12 m^2/g while the untreated sample had only 4.23 m^2/g. This stabilization of the surface area can be attributed to the hydrothermal treatment of the precursors. Previous studies on hydrous zirconia showed that temperature, pH of the medium and length of hydrothermal treatment can affect the surface area, porosity and thermal stability of the resulting zirconia [43–46]. It was postulated that as a result of the high temperatures during hydrothermal synthesis, collisions between primary particles are enhanced [44]. Condensation of surface hydroxyl groups leads to the formation of a porous network of particles, which is further

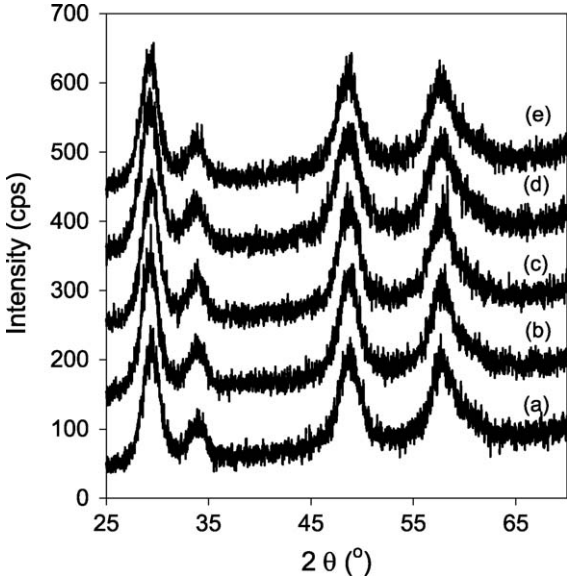

Fig. 3. XRD of 500 °C-calcined $Ce_{0.5}Zr_{0.5}O_2$ prepared by hydrothermal synthesis for (a) 0, (b) 1, (c) 2, (d) 4 and (e) 8 days.

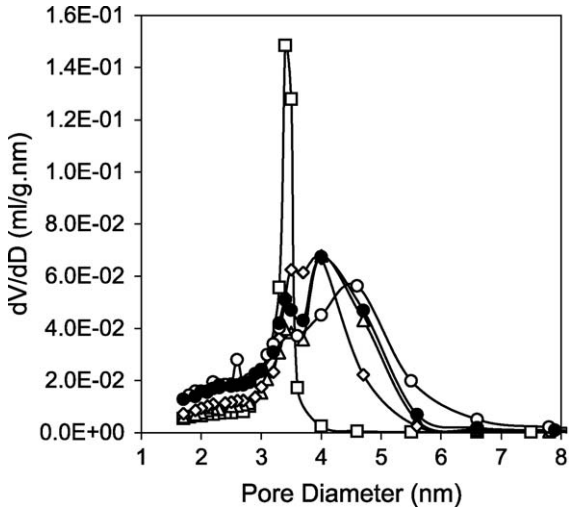

Fig. 4. Pore size distribution of $Ce_{0.5}Zr_{0.5}O_2$ prepared by hydrothermal synthesis for (□) 0, (△) 1, (◇) 2, (○) 4 and (●) 8 days.

strengthened by the continuous dissolution and reprecipitation of material under hydrothermal conditions. The pH of the reaction medium determines the solubility of the hydrous oxide and hence, the extent of dissolution and reprecipitation of the material [45]. Deposition at the neck areas adjoining particles reinforces the network and helps it to withstand capillary forces during drying and calcination to high temperatures. The thermal stability of the hydrothermally treated samples may be due to the decrease or elimination of defect sites such as Schottky defects which are believed to be responsible for sintering of particles [56]. Di Monte et al. [57] found that thermal stability to 1000 °C depends on the development of a high degree of crystallinity, a decrease of particle size, as well as the formation of mesopores with diameters greater than 7 nm during hydrothermal treatment of the cerium–zirconium hydroxides.

3.4. Oxygen storage capacity of hydrothermally treated $Ce_{0.5}Zr_{0.5}O_2$

In addition to higher surface area and better thermal stability, the hydrothermal treatment also influenced the reducibility of $Ce_{0.5}Zr_{0.5}O_2$. Untreated $Ce_{0.5}Zr_{0.5}O_2$ was reduced between 180 and 650 °C, with the maximum CO_2 desorption at 450 °C (Fig. 6a). Although ceria–zirconia samples prepared from hydrothermally

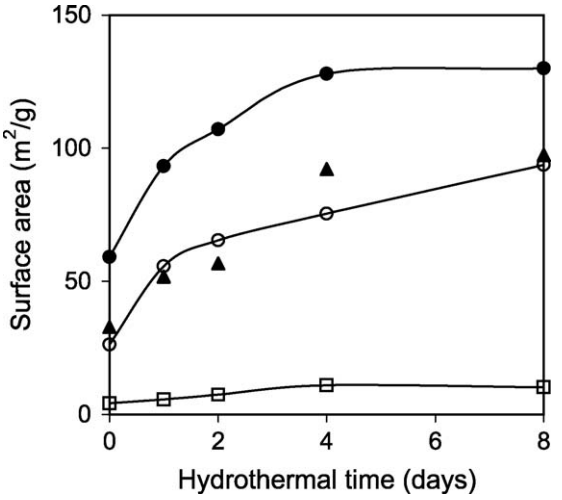

Fig. 5. Surface area of hydrothermally treated $Ce_{0.5}Zr_{0.5}O_2$ after calcination at (●) 500 °C, (▲) 700 °C, (□) 1000 °C and (○) after redox reactions.

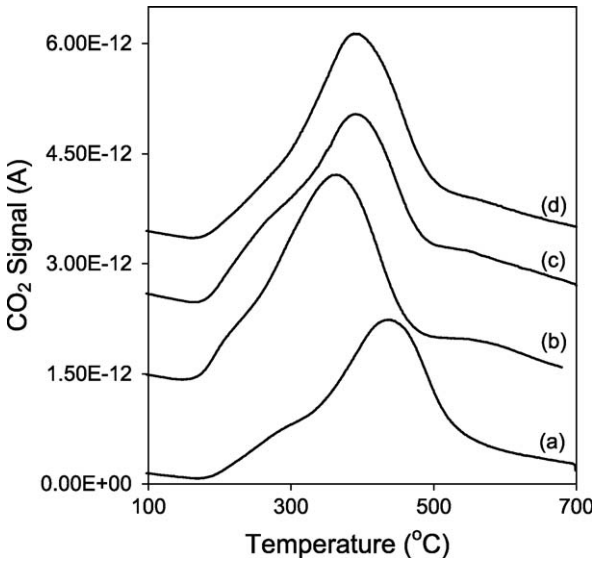

Fig. 6. CO_2 signal during TPR of $Ce_{0.5}Zr_{0.5}O_2$ hydrothermally treated for (a) 0, (b) 1, (c) 4 and (d) 8 days.

treated precursors were reduced within the same temperature range, the peak maximum was shifted to lower temperatures between 368 and 400 °C (Fig. 6b–d). The higher surface area of these samples allows more gas–surface interaction, thus facilitating the removal of oxygen. The OSC was of the hydrothermally treated samples was slightly higher (0.57–0.59 mmol O_2/g) than that of the untreated oxide, 0.50 mmol O_2/g (Table 2).

3.5. Effect of silica doping on $Ce_{0.5}Zr_{0.5}O_2$

The effect of silica was examined by subjecting cerium–zirconium hydroxides (Ce:Zr 1:1) to 4 days of hydrothermal treatment at 100 °C in the presence of different concentrations of tetraethylorthosilicate. The X-ray diffraction peaks of the samples after calcination at 500 °C were of lower intensity and broader than the silica-free samples (Fig. 7). The crystallite size was calculated to be in the range of 3.3–4.2 nm, which is smaller than that of the pure ceria–zirconia, 5.5 nm (Table 3). However, no diffraction peaks of

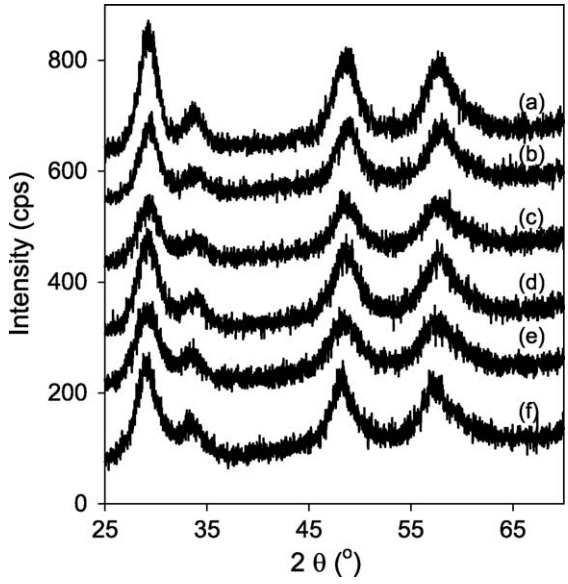

Fig. 7. XRD patterns (a) CZ-H-4, (b) 1%Si-CZ-H-4, (c) 2%Si-CZ-H-4, (d) 4%Si-CZ-H-4, (e) 5%Si-CZ-H-4 and (f) 10%Si-CZ-H-4.

Table 3
Textural properties of silica-loaded ceria–zirconia.

Sample	Surface area (m^2/g)				Si (wt.%)[a]	Crystallite size (nm)	
	500 °C	700 °C	After TPR	1000 °C		Before TPR	After TPR
0%Si-CZ-H-4	128	92.2	75.4	10.9	–	5.5	7.4
1%Si-CZ-H-4	140	102	99.0	1.85	1.13	4.2	4.7
2%Si -CZ-H-4	142	114	113	1.88	2.04	4.2	5.6
3%Si-CZ-H-4	145	125	126	1.73	3.15	4.2	4.4
4%Si-CZ-H-4	171	135	136	2.40	3.87	4.2	4.8
5%Si-CZ-H-4	175	152	140	2.04	4.73	3.8	4.5
7.5%-Si-CZ-H-4	184	158	154	3.30	5.50	3.3	3.9
10%Si-CZ-H-4	199	168	160	2.31	5.98	4.3	4.8
4%Si-CZ-H-0	141	96.0	99.0	1.05	3.03	4.2	4.9
4%Si-CZ-H-1	201	139	142	–	3.80	4.3	4.6
4%Si-CZ-H-2	181	130	130	–	3.94	4.3	4.7
4%Si-CZ-H-4	182	138	147	2.80	4.05	4.3	4.6
4%Si-CZ-H-8	185	149	148	2.18	4.14	4.4	4.8

[a] From ICP-AES.

silica were observed even for the highest Si loading. The slight shift to lower angles with increasing Si content may be attributed to the incorporation of silicon in the interstitial sites of the crystal structure. The amount of silica incorporated in the samples was quantified using ICP analyses. For Si loadings $\leq$5 wt.%, the amount incorporated agreed very well with the expected loading. However, for the higher loadings of 7.5 and 10 wt.% Si, only 5.50 and 5.98 wt.% Si was found, respectively.

Two effects were observed for the silica-doped ceria–zirconia, namely (i) an increase in the surface area and (ii) higher resistance to sintering and stabilization of the surface area up to 700 °C. For 0%Si-CZ-H-4, the surface area was 128 m^2/g but it increased to 199 m^2/g in 10%Si-CZ-H-4 (Table 3). This dependence of surface area on silica differs from that observed for silica-doped materials prepared by flame spray pyrolysis. In the latter samples, it was reported that the specific surface area remained constant, at around 93 m^2/g, for silica loadings between 0 and 1.2 wt.% but decreased slightly to 86 m^2/g for higher loadings of 3–6 wt.% silica (1.4–2.9 wt.% Si) [47]. The difference in the observations may be due to the high temperatures present in the flame synthesis of the oxides. In the present study, the samples were prepared by hydrothermal synthesis, and even after calcination at 700 °C for 12 h, the surface area remained high, ranging from 92 m^2/g in 0%Si-CZ-H-4 to 168 m^2/g in 10%Si-CZ-H-4 (Table 3). The ability to retain a high surface area despite higher calcination temperature shows that Si is a good dopant for textural stabilization.

The OSC for ceria–zirconia with 1–5 wt.% Si was higher than for the undoped sample but oxides with even higher Si loading had smaller OSC even after correcting for the decreased concentration of ceria–zirconia in the latter samples (Table 2). Hence, an intermediate silica loading is beneficial for an enhancement in the OSC of ceria–zirconia. The positive effect of Si doping on the OSC has been observed before, although the reported optimum dopant level varies. For $Ce_{0.5}Zr_{0.5}O_2$ synthesized by flame spray pyrolysis, Schulz et al. [47] found an enhanced OSC for silica loadings up to 3 wt.% SiO_2 (1.4 wt.% Si). Rocchini et al. [14] reported the formation of amorphous silica and nanocrystalline ceria following high temperature redox treatment of ceria with more than 3 wt.% Si. The authors correlated this to the promotion of oxygen storage. However, examination of the used samples in this study did not show the presence of any ceria.

3.6. Effect of hydrothermal treatment on silica-containing ceria–zirconia

The effect of hydrothermal treatment on 4 wt.% Si-containing cerium–zirconium hydroxides was investigated. Elemental analyses on the calcined $Si/Ce_{0.5}Zr_{0.5}O_2$ samples showed that the Si concentration in the samples increased slightly with the length of hydrothermal synthesis (Table 3). Under the alkaline conditions of the hydrothermal synthesis, tetraethylorthosilicate is hydrolyzed to the soluble $Si(OH)_4$. The longer the precipitate is exposed to the mother liquor, the more silicon that can be taken up. The X-ray diffractograms of the calcined oxides showed peaks of low intensity corresponding to the cubic fluorite phase. No silica phase could be detected in the samples. The crystallite size was determined to be between 4.2 and 4.4 nm which is smaller than in the pure ceria–zirconia samples. Due to the presence of silica, the untreated oxide, 4%Si-CZ-H-0, had a high surface area of 141 m^2/g after calcination to 500 °C (Table 3). Similar to the pure ceria–zirconia, hydrothermal treatment of the precursors further increased the surface area of the resulting oxides to 181–201 m^2/g. The hydrothermally treated samples retained surface areas of 130–149 m^2/g after calcination at 700 °C. In contrast, the surface area of the untreated 4%Si-CZ-H-0 decreased to 96 m^2/g.

The CO reduction of the 4%Si-CZ-H-O occurred above 250 °C with the peak maximum shifting to higher temperatures for the hydrothermally treated samples (Fig. 8). Compared with the CZ-H-series, the asymmetry of the desorption peaks was less pronounced for the silica-containing samples. This, together with the later onset of reduction, suggests that less oxygen was removed from the surface layers than in the silica-free samples. Indeed the OSC of

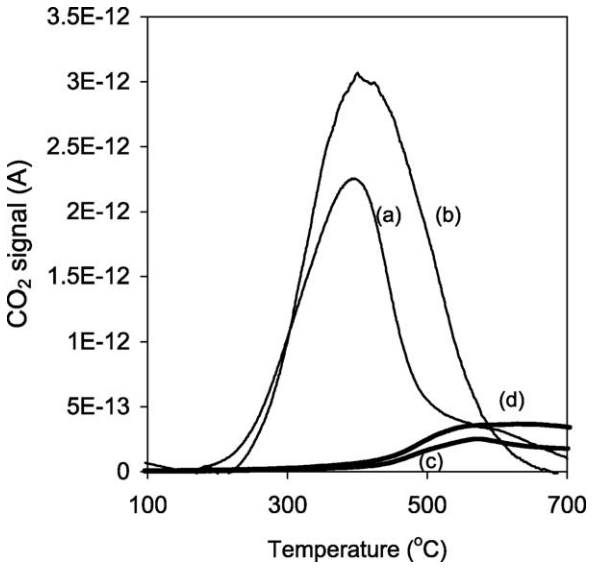

Fig. 8. CO_2 signal during TPR of (a and c) 4%Si-CZ-H-0 and (b and d) 4%Si-CZ-H-8 calcined at 500 and 1000 °C, respectively.

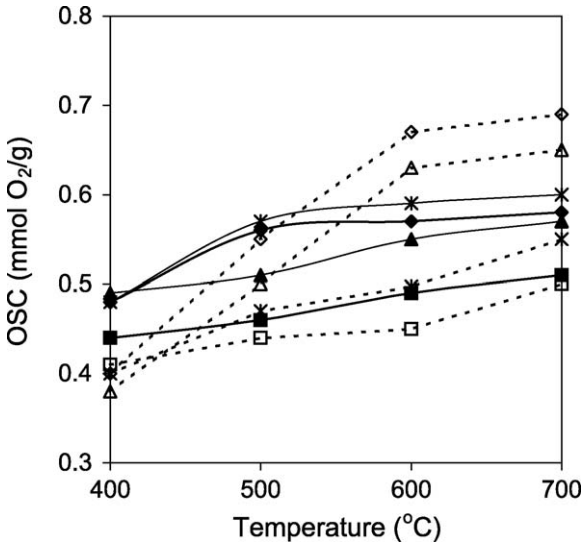

Fig. 9. Oxygen storage capacity at different temperatures for CZ-H (full lines) and 4%Si-CZ-H (dotted lines) hydrothermally treated for 0 (■, □); 1 (✱); 4 (▲, △); and 8 days (◆, ◇).

the silica-doped samples at 400 and 500 °C was lower than that of the undoped samples (Fig. 9). The presence of silica may block sites required for adsorption of CO or hinder oxygen migration. However, at higher temperatures of 600 °C and above, the 4- and 8-day hydrothermally treated silica-doped samples had higher OSC than those subjected to shorter hydrothermal treatment or that were silica-free. The OSC values of 0.65–0.69 mmol O_2/g indicates that about 77–80% of the cerium can be reversibly reduced and reoxidized.

3.7. Effect of high temperature calcination and surface area on oxygen storage capacity

After calcination at 1000 °C for 12 h, the untreated CZ-H-0 sample had a surface area of 4.23 m^2/g while the hydrothermally treated silica-free CZ samples retained 9–12 m^2/g. The latter values are similar to that reported by Si et al. [29] for ceria–zirconia doped with rare earth metals like praseodymium and neodymium. In contrast, the surface area of silica-doped ceria–zirconia decreased tremendously to 1.0–2.8 m^2/g after calcination at 1000 °C. This is despite their ability to maintain high surface areas when calcined at 700 °C. The powder X-ray diffractograms obtained after thermal treatment at 1000 °C showed no observable phase changes aside from an increase in crystallinity of the samples (Fig. 10). The crystallite sizes of the silica-doped ceria–zirconia were between 13 and 15 nm, a threefold increase from the 700 °C-treated samples. In comparison, smaller crystallite sizes of 10–11 nm were found for the silica-free ceria–zirconia. Hence, the drastic loss in surface area of the 1000 °C-treated samples can be attributed to enhanced grain growth/sintering.

The TPR curves of the 1000 °C-calcined samples were shifted to higher temperatures compared to samples calcined at 500 °C (Figs. 8 and 11). This may be partly attributed to the lower surface area as sites for CO adsorption becomes limiting. Furthermore, as larger crystallites formed due to sintering, the diffusion path for the migration of bulk oxygen to the surface is increased. However, despite an almost 10-fold decrease in surface area, the OSC of CZ-H-0 and CZ-H-4 was only reduced by half to 0.22–0.26 mmol O_2/g (Fig. 12A). The OSC for silica-containing 4%Si-CZ-H-0 and 4%Si-CZ-H-8 was even smaller, 0.07 and 0.1 mmol O_2/g, respectively. X-ray photoelectron spectroscopy showed that the surface Si concentration was higher after calcination at 1000 °C than at 500 °C (Fig. 12B). In 4%Si-CZ-H-0, the Si/(Si + Zr + Ce) increased from 0.10 to 0.37 (Table 4). Furthermore, the binding energy of the Si 2p peak was shifted from 101.4 to 102.5 eV, indicating a change in the composition of the surface oxides [58–60]. Indeed, after calcination the surface was enriched with zirconium. The surface Zr/Ce ratio was 1.09 in the sample calcined at 500 °C, and this ratio increased to 1.95 after calcination at 1000 °C. The result suggests that after the calcination at 1000 °C, a surface overlayer of a zirconium-rich silicate phase is formed, which could contribute to the reduction in surface area and the oxygen storage capacity. Aside from surface segregation, analysis of the bulk oxides by XRD showed no phase change in the 1000 °C-aged samples (Fig. 10).

Contrary to expectation, a high surface area is not the determining quantity for good reversible oxygen storage. In this work, ceria–zirconia with various surface areas could be synthesized by varying the hydrothermal time. Our results show that materials with surface areas less than 50 m^2/g had smaller OSC values than those with higher surface areas (Fig. 13). However, the

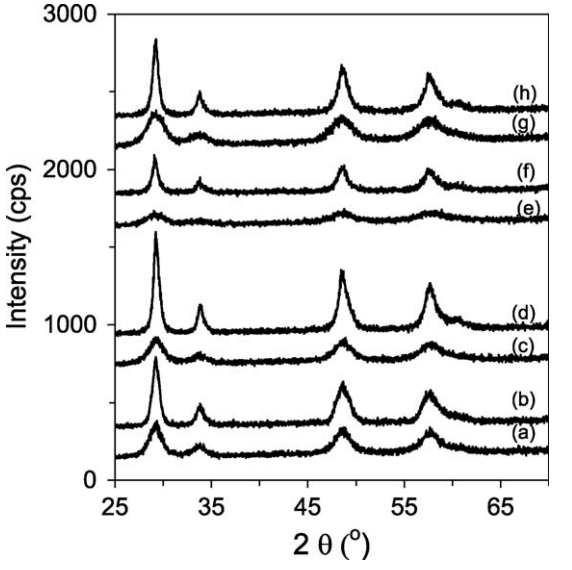

Fig. 10. X-ray diffractograms of (a and b) CZ-H-0, (c and d) CZ-H-4, (e and f) 4%Si-CZ-H-0 and (g and h) 4%Si-CZ-H-8 after calcination at 700 and 1000 °C, respectively.

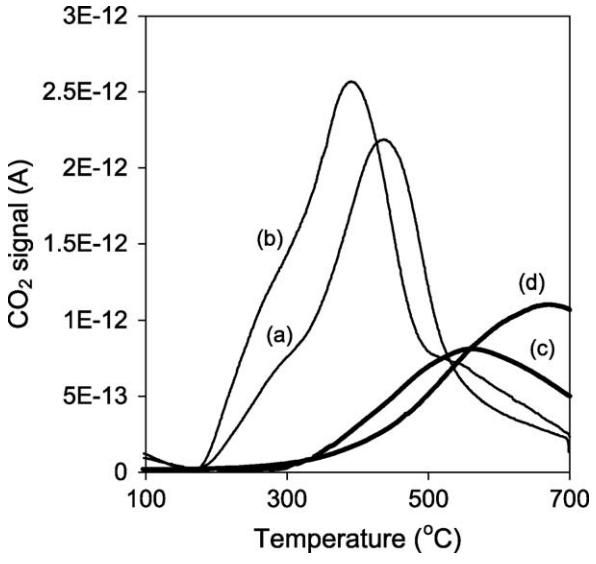

Fig. 11. CO_2 signal during TPR of (a and c) CZ-H-0 and (b and d) CZ-H-4 calcined at 500 and 1000 °C, respectively.

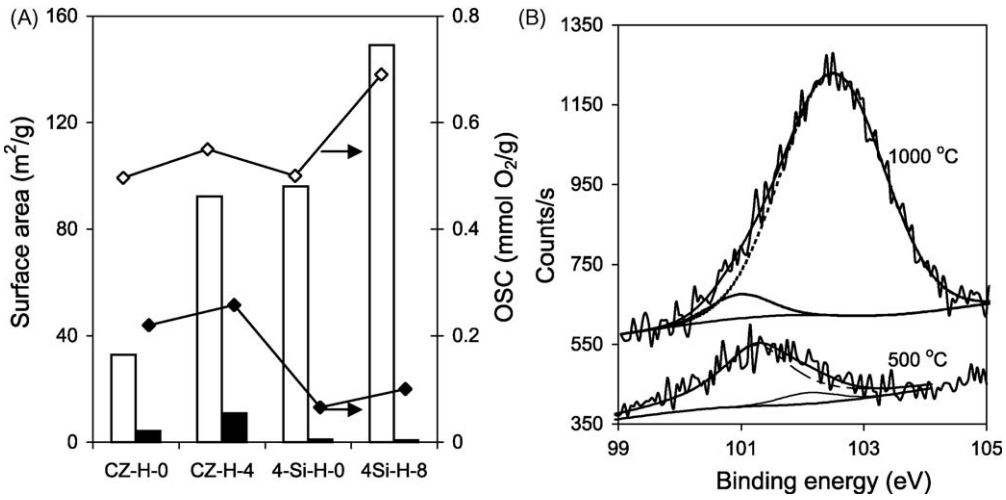

Fig. 12. (A) Surface area and OSC after calcination at 500 °C (open symbols) and 1000 °C (filled symbols). (B) Si 2p XPS spectra of 4%Si-CZ-H-0 after calcination at 500 °C and 1000 °C.

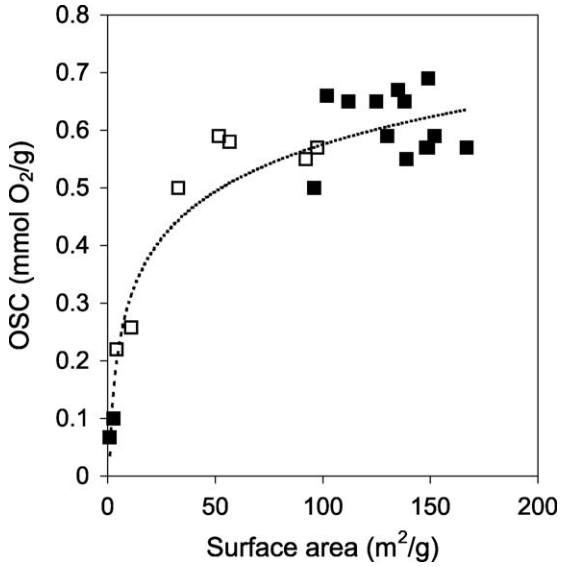

Fig. 13. OSC at 700 °C vs. surface area of ceria–zirconia. (□) CZ-H and (■) Si-CZ-series.

OSC does not increase proportionally with the surface area and remains between 0.5 and 0.7 mmol O_2/g for surface areas above 50 m^2/g. This shows that below 50 m^2/g, the oxygen exchange is limited by the surface and the OSC increases proportionately with surface area. However, for oxides with high surface area, oxygen from the bulk contributes substantially to the amount of reversibly exchanged oxygen, and a limiting amount is expected for very small crystallites where the entire material becomes completely reduced. The ease of oxygen removal in the hydrothermally synthesized samples (as indicated by an earlier onset temperature in TPR) could be due to better atomic mixing as a result of dissolution and reprecipitation of the cerium–zirconium hydroxide during hydrothermal treatment. This is in line with the hypothesis of Nagai et al. [24] that atomic homogeneity plays an important role in OSC. These authors observed that a CeO_2–ZrO_2 sample with a very low surface area of 1 m^2/g had an OSC of 1.5 mmol-O/g, whereas another sample with 125 m^2/g had an OSC of only 0.16 mmol-O/g. Likewise, Mamontov et al. [61] found that the OSC did not correlate with the surface area or the crystallite size but rather with the size of intracrystallite domains enriched in zirconia. Oxygen located at the interface between the zirconia-rich and ceria-rich domains is postulated to be responsible for the OSC. The highest OSC was associated with small domain sizes, irrespective of the size of the crystallite. Si et al. [29] observed that the OSC does not depend strongly on the grain size, surface area or microstrain. However, the surface areas considered were lower, between 5 and 20 m^2/g.

Table 4
XPS results of 4%Si-CZ samples calcined at 500 and 1000 °C.

Sample	Binding energy	XPS atomic ratio[a]	
	Si 2p	Zr/Ce	Si/(Si + Ce + Zr)
4%Si-CZ-H-0-500 °C	101.4	1.09	0.10
4%Si-CZ-H-0-1000 °C	102.5	1.95	0.37
4%Si-CZ-H-8-500 °C	101.4	1.17	0.08

[a] Calculated using atomic sensitivity factors: Ce 3d (6.5), Zr 3d (1.8) and Si 2p (0.4).

4. Conclusions

The surface area and porosity of pure and silica-doped ceria–zirconia increased with the length of hydrothermal treatment. These samples showed good thermal stability and structural integrity even after repeated redox cycles at 700 °C. These hydrothermally treated samples were also more reducible as oxygen could be removed at a lower temperature than for the untreated ceria–zirconia. The addition of silica to ceria–zirconia resulted in higher surface areas. However, the thermal stability and OSC of these samples after calcination at 1000 °C was lower than pure hydrothermally treated ceria–zirconia. From XPS studies, the surface regions of the silica-doped samples were found to be enriched in Si and Zr after the high temperature calcination. The OSC shows a strong dependence on surface area for ceria–zirconia with less than 50 m^2/g but for high surface area oxides, the amount of exchangeable oxygen is limited by the intrinsic reducibility of the material. The amount of reversibly exchangeable oxygen is as high as 80% of the theoretical capacity, assuming that all cerium can be reduced from the +4 to the +3 state, whereas Zr^{4+} does not change its oxidation state.

Acknowledgements

We thank the National University of Singapore for financial support under grant R-143-000-329-112 as well as the award of a research scholarship to V. Raju.

References

[1] T. Kanazawa, Catal. Today 96 (2004) 171.
[2] A. Trovarelli, Catalysis by Ceria and Related Materials, Catalytic Science Series 2, World Scientific, London, 2002.
[3] S. Bernal, J. Kasper, A. Trovarelli, Catal. Today 50 (1999) 173.
[4] R.K. Usmen, G.W. Graham, W.L.H. Watkins, R.W. McCabe, Catal. Lett. 30 (1995) 53.
[5] A. Bensalem, F. Bozon-Verduraz, M. Delamar, G. Bugli, Appl. Catal. A 121 (1995) 81.
[6] F. Zamar, A. Trovarelli, C. de Leitenburg, G. Dolcetti, Chem. Commun. (1995) 965.
[7] G. Dutta, U.V. Waghmare, T. Baidya, M.S. Hedge, K.R. Priolkar, P.R. Sarode, Chem. Mater. 18 (2006) 3249.
[8] M. Haneda, T. Mizushima, N. Kakuta, J. Phys. Chem. B 102 (1998) 6579.
[9] B.M. Reddy, A. Khan, P. Lakshmanan, M. Aouine, S. Loridant, J.-C. Volta, J. Phys. Chem. B 109 (2005) 3355.
[10] M.H. Yao, R.J. Baird, F.W. Kunz, T.E. Hoost, J. Catal. 166 (1997) 67.
[11] S. Damyanov, C.A. Perez, M. Schmal, J.M.C. Bueno, Appl. Catal. A 234 (2002) 271.
[12] M. Sugiura, Catal. Surv. Asia 7 (2003) 77.
[13] M. Ozawa, K. Matsuda, S. Suzuki, J. Alloys Compd. 303–304 (2000) 56.
[14] E. Rocchini, A. Trovarelli, J. Llorca, G.W. Graham, W.H. Weber, M. Maciejewski, A. Baiker, J. Catal. 194 (2000) 461.
[15] M. Pijolat, M. Prin, M. Soustelle, O. Touret, P. Nortier, J. Chem. Soc., Faraday Trans. 91 (1995) 3941.
[16] P. Fornasiero, E. Fonda, R. Di Monte, G. Vlaic, J. Kašpar, M. Graziani, J. Catal. 187 (1999) 177.
[17] G. Vlaic, P. Fornasiero, S. Geremia, J. Kašpar, M. Graziani, J. Catal. 168 (1997) 386.
[18] A. Trovarelli, F. Zamar, J. Llorca, C. de Leitenburg, G. Dolcetti, J.T. Kiss, J. Catal. 169 (1997) 490.
[19] P. Fornasiero, G. Balducci, R. Di Monte, J. Kašpar, V. Sergo, G. Gubitosa, A. Ferrero, M. Graziani, J. Catal. 164 (1996) 173.
[20] S. Lemaux, A. Bensaddik, A.M.J. van der Ewrden, J.H. Bitter, D.C. Koningsberger, J. Phys. Chem. B 105 (2001) 4810.
[21] M. Daturi, E. Finocchio, C. Binet, J.-C. Lavalley, F. Fally, V. Perrichon, H. Vidal, N. Hickey, J. Kašpar, J. Phys. Chem. B 104 (2000) 9186.
[22] R. Di Monte, J. Kašpar, J. Mater. Chem. 15 (2005) 633.
[23] E. Mamontov, T. Egami, R. Brezny, M. Koranne, S. Tyagi, J. Phys. Chem. B 104 (2000) 11110.
[24] Y. Nagai, T. Yamamoto, T. Tanaka, S. Yoshida, T. Nonaka, T. Okamoto, A. Suda, M. Sugiura, Catal. Today 74 (2002) 225.
[25] P. Vidmar, P. Fornasiero, J. Kašpar, G. Gubitosa, M. Graziani, J. Catal. 171 (1999) 160.
[26] H. He, H.X. Dai, K.W. Wong, C.T. Au, Appl. Catal. A 251 (2003) 61.
[27] R. Di Monte, P. Fornasiero, S. Desinan, J. Kašpar, J.M. Gatica, J.J. Calvino, E. Fonda, Chem. Mater. 16 (2004) 427.
[28] T. Masui, T. Ozaki, K. Machida, G. Adachi, J. Alloys Compd. 303–304 (2000) 49.
[29] R. Si, Y.W. Zhang, L.M. Wang, S.J. Li, B.X. Lin, W.S. Chu, Z.Y. Wu, C.H. Yan, J. Phys. Chem. C 111 (2007) 787.
[30] A. Morikawa, T. Suzuki, T. Kanazawa, K. Kikuta, A. Suda, H. Shinjo, Appl. Catal. B 78 (2008) 210.
[31] C.E. Hori, H. Permana, K.Y. Ng, A. Brenner, K. More, K.M. Rahmoeller, D. Belton, Appl. Catal. B 16 (1998) 105.
[32] C. Bozo, N. Guilhaume, E. Garbowski, M. Primet, Catal. Today 59 (2000) 33.
[33] S. Rossignol, Y. Madier, D. Duprez, Catal. Today 50 (1999) 261.
[34] A. Martínez-Arias, M. Fernández-García, V. Ballesteros, L.N. Salamanca, J.C. Conesa, C. Otero, J. Soria, Langmuir 15 (1999) 4796.
[35] C. de Leitenburg, A. Trovarelli, F. Zamar, S. Maschio, G. Dolcetti, J. Llorca, Chem. Commun. (1995) 2181.
[36] J.R. Kim, W.J. Myeong, S.K. Ihm, Appl. Catal. B 71 (2007) 57.
[37] W.J. Stark, M. Maciejewski, L. Mädler, S.E. Pratsinis, A. Baiker, J. Catal. 220 (2003) 35.
[38] T. Masui, K. Nakano, T. Ozaki, G.-Y. Adachi, Z. Kang, L.R. Eyring, Chem. Mater. 13 (2001) 1834.
[39] R. Di Monte, P. Fornasiero, J. Kašpar, M. Graziani, J.M. Gatica, S. Bernal, A. Gŏmez-Herrero, Chem. Commun. (2000) 2167.
[40] A.I. Kozlov, D.H. Kim, A. Yezerets, P. Anderson, H.H. Kung, M.C. Kung, J. Catal. 209 (2002) 417.
[41] B.M. Reddy, P. Lakshmanan, A. Khan, S. Loridant, C.L. Cartes, T.C. Rojas, A. Fernandez, J. Phys. Chem. B 109 (2005) 13545.
[42] B.M. Reddy, P. Saikia, P. Bharali, L. Katta, G. Thrimurthulu, Catal. Today 141 (2009) 109.
[43] G.K. Chuah, S. Jaenicke, S.A. Cheong, K.S. Chan, Appl. Catal. A 145 (1996) 267.
[44] G.K. Chuah, Catal. Today 49 (1999) 131.
[45] G.K. Chuah, S. Jaenicke, B.K. Pong, J. Catal. 175 (1998) 80.
[46] S. Jaenicke, G.K. Chuah, V. Raju, Y.T. Nie, Catal. Surv. Asia 12 (2008) 153.
[47] H. Schulz, W.J. Stark, M. Maciejewski, S.E. Pratsinis, A. Baiker, J. Mater. Chem. 13 (2003) 2979.
[48] M. Zhao, M. Shen, J. Wang, J. Catal. 248 (2007) 258.
[49] J. Kašpar, R. Di Monte, P. Fornasiero, M. Graziani, H. Bradshaw, C. Norman, Top. Catal. 16/17 (2001) 83.
[50] VG Scientific Technical Document TD 8618.
[51] R.D. Shannon, Acta Cryst. A32 (1976) 751.
[52] A.R. West, Solid State Chemistry and its Applications, John Wiley & Sons, Wiltshire, 1984.
[53] S.J. Gregg, K.S.W. Sing, Adsorption, Surface Area and Porosity, Academic Press, London, 1982.
[54] C. Li, Y. Skata, T. Arai, K. Domen, K. Maruya, T. Onishi, Chem. Commun. (1991) 410.
[55] N. Kakuta, S. Ikawa, T. Eguichi, K. Murakami, H. Ohkita, T. Mizuhima, J. Alloys Compd. 408–412 (2006) 1078.
[56] P.D.L. Mercera, J.G. van Ommen, E.B.M. Doesburg, A.J. Burggraaf, J.R.H. Ross, Appl. Catal. 78 (1991) 79.
[57] R. Di Monte, J. Kašpar, H. Bradshaw, C. Norman, J. Rare Earths 26 (2008) 136.
[58] H. Behner, J. Wecker, T. Mattheel, K. Samwer, Surf. Interface Anal. 18 (1992) 685.
[59] B.M. Reddy, P. Lakshmanan, P. Bharali, P. Saikia, J. Mol. Catal. A 258 (2006) 355.
[60] A.T.S. Wee, Z.C. Feng, H.H. Hng, K.L. Tan, C.C. Tin, R. Hu, R. Coston, Appl. Surf. Sci. 81 (1994) 377.
[61] E. Mamontov, R. Brezny, M. Koranne, T. Egami, J. Phys. Chem. B 107 (2003) 13007.